Carbohydrate Polymers 94 (2013) 420–429

Contents lists available at SciVerse ScienceDirect

Carbohydrate Polymers

journal homepage: www.elsevier.com/locate/carbpol

Galactosylated chitosan–polycaprolactone nanoparticles for hepatocyte-targeted delivery of curcumin

Nuo Zhou[a,1], Xiaoli Zan[b,1], Zheng Wang[c], Hua Wu[d,*], Dengke Yin[b], Chunyan Liao[b], Ying Wan[b,**]

[a] The Affiliated Stomatology Hospital, Guangxi Medical University, Nanning 530021, PR China
[b] College of Life Science and Technology, Huazhong University of Science and Technology, Wuhan 430074, PR China
[c] School of Pharmaceutical Science and Technology, Tianjin University, Tianjin 300072, PR China
[d] Department of Nuclear Medicine and Minnan PET Center, The First Affiliated Hospital of Xiamen University, Xiamen 316003, PR China

ARTICLE INFO

Article history:
Received 21 November 2012
Received in revised form 5 January 2013
Accepted 8 January 2013
Available online 16 January 2013

Keywords:
Chitosan copolymer
Nanoparticle
Curcumin
Hepatocyte-targeted characteristic
Drug delivery

ABSTRACT

Galactosylated chitosan–polycaprolactone (Gal-CH–PCL) copolymers with a galactosylation degree of around 10% and varied PCL percentages less than 40 wt% were synthesized and used to produce nanoparticles for delivering curcumin. Some nanoparticles with encapsulation efficiency of 70% or higher and sizes changing from 100 to 250 nm were able to deliver curcumin in a controlled manner. PCL content in Gal-CH–PCLs was found to be a key factor for governing the release behavior of nanoparticles. Hepatocyte-targeted characteristic of nanoparticles was confirmed using human hepatocellular carcinoma (HepG2) cells. In comparison to free curcumin, curcumin-loaded Gal-CH–PCL nanoparticles well retained its anticancer activity. At an equivalent curcumin-dose of around 20 μg/mL that was found to be relatively safe to human normal liver cells, the results obtained from flow-cytometry revealed that some optimized Gal-CH–PCL nanoparticles showed more than 6-fold increasing abilities to induce the apoptosis and necrosis of HepG2 cells during 72 h treatment compared to free curcumin.

© 2013 Elsevier Ltd. All rights reserved.

1. Introduction

Chemotherapy involved in different cancers is often associated with some drawbacks such as nonselective distribution of drugs, drug toxicity and unwanted side effects to normal tissues (Chen et al., 2009; Das, Mohanty, & Sahoo, 2009). In addition, most of currently available anticancer agents usually have short circulation half life in plasma and poor aqueous solubility, and thus, their therapeutic efficacy is limited to a certain extent (Liang et al., 2006). To date, different types of synthetic and natural anticancer drugs have been used for chemotherapy. Of many natural anticancer drugs, curcumin has drawn increasing attention since it can sensitize cancer cells and induce apoptosis or even death of the sensitized cancer cells (Aggarwal, Kumar, & Bharti, 2003). Curcumin is a hydrophobic polyphenol derivative extracted from natural herbal and it has diverse biological properties. In particular, curcumin is relatively safe to normal tissues in a certain dose range (Aggarwal & Sung, 2009). Many reports reveal that curcumin has big potential in reducing the chance of lung cancer and colon cancer, and it has also been taken as an imminent herbal drug for treatment of other cancers (Anand et al., 2008). Nevertheless, the satisfactory pharmaceutical efficacy of curcumin is hard to achieve even at high dosage because curcumin is extremely lack of solubility in aqueous media and it can be rapidly degraded under physiological conditions (Anand, Kunnumakkara, Newman, & Aggarwal, 2007; Mohanty & Sahoo, 2010). Some biodegradable polymer nanoparticles have thus been used as vehicles to protect curcumin from degradation or elimination in circulatory system while delivering curcumin at or around cancer tissues (Das, Kasoju, & Bora, 2010; Mohanty & Sahoo, 2010).

It is known that nanoparticles can enter tumor sites via either passive or active targeting approaches. Some reports indicate that polymer nanoparticles having a size of around 200 nm permit efficient accumulation in tumor tissues via passive uptake or enhanced permeability and retention (EPR) effect (Acharya & Sahoo, 2011). As regards active targeting delivery, one of effective approaches is to utilize some ligand-receptor interactions. Up to now, many studies have been conducted to functionalize polymer nanoparticles for enhanced active targeting features (Chan et al., 2009; Ganta, Devalapally, Shahiwala, & Amiji, 2008; Greco & Vicent, 2009; Lu et al., 2011). In the case of hepatocyte-targeted delivery systems, some polymers attached with galactosylated or lactosylated conjugates have been used to prepare nanoparticles for active targeting delivery of anticancer drugs because asialoglycoprotein receptors on hepatoma cells can specifically bind with certain types

* Corresponding author.
** Corresponding author. Tel.: +86 27 87792147; fax: +86 27 87792234.
E-mail addresses: wuhua1025@163.com (H. Wu), ying_x_wan@yahoo.ca (Y. Wan).
[1] These authors contributed equally to this work.

0144-8617/$ – see front matter © 2013 Elsevier Ltd. All rights reserved.
http://dx.doi.org/10.1016/j.carbpol.2013.01.014

of ligands containing specific terminals such as β-D-galactose and *N*-acetylgalactosamine residues (Wang et al., 2006; Wu, Nantz, & Zern, 2002).

Chitosan, a partially *N*-deacetylated derivative of chitin, has many enticing properties such as biodegradability, hydrophilicity, anti-microbial activity, bioadherence and cell affinity (Kumar, Muzzarelli, Muzzarelli, Sashiwa, & Domb, 2004; Muzzarelli, 2009; Muzzarelli, Greco, Busilacchi, Sollazzo, & Gigante, 2012). Several types of lactosaminated or galactosylated chitosan derivatives have been reported for the applications in hepatocyte-specific carriers (Agnihotri, Mallikarjuna, & Aminabhavi, 2004). In addition, some galactosylated chitosan copolymers with hepatocyte-targeted characteristics have also been investigated for applications in gene vectors (Park et al., 2000). Although chitosan and some its derivatives have been used for delivering curcumin (Anitha et al., 2011a, 2011b; Das et al., 2010), chitosan nanoparticles usually have a very low initial load for hydrophobic curcumin and show severe burst release characteristics. To endue chitosan nanoparticles with enhanced ability to more efficiently load curcumin and to release curcumin in a well-controlled manner, new types of chitosan-based carriers are still worthy of exploring.

Grafting polycaprolactone side chains onto chitosan backbone may generate some proper chitosan–polycaprolactone (CH–PCL) copolymers that can be used as nanoparticle carriers for delivering water-insoluble curcumin with enhanced bioavailability due to the amphiphilic properties of CH–PCLs. In addition, CH–PCLs can also be galactosylated to achieve hepatocyte-targeted specificity for the resulting CH–PCL nanoparticles. To our knowledge, little effort has been made to build such hepatocyte-targeted CH–PCL nanoparticles for curcumin delivery, and thus, in the present study, galactosylated CH–PCLs were synthesized, and curcumin-loaded galactosylated CH–PCL nanoparticles were examined for possible applications in hepatocyte-targeted delivery of curcumin.

2. Experimental

2.1. Materials

Chitosan was supplied by Aladdin Inc. 3-(4,5-Dimethylthiazol-2-yl)-2,5-diphenyltetrazolium bromide (MTT) and lactobionic acid (LA) were purchased from Amresco. Caprolactone and 2-(*N*-morpholino)ethanesulfonic acid sodium salt were purchased from Sigma–Aldrich. Microporous membrane tubing with various molecular weight cut-off (MWCO) values changing from 3.5 to 300 kDa was obtained from Spectrum Laboratories Inc. 1-ethyl-3-(3-dimethylaminopropyl) carbodiimide hydrochloride, curcumin and *N*-hydroxylsuccinimide were purchased from Sinopharm Chemical Reagent Inc. All other chemicals were bought from different companies in China and they were of analytical grade.

Highly deacetylated chitosan was obtained by deacetylating chitosan with 50 wt% NaOH solution. Degree of deacetylation and viscosity average molecular weight of chitosan were measured as $95.4 \pm 1.7\%$ and $2.68 \pm 0.31 \times 10^4$, respectively, following reported methods (Wan, Creber, Peppley, & Bui, 2004).

2.2. Synthesis of galactosylated chitosan and galactosylated chitosan–polycaprolactone

Galactosylated chitosan (Gal-CH) was synthesized following a method describe elsewhere (Kim, Park, Nah, Choi, & Cho, 2004). The resulting products were dialyzed (MWCO = 5000) against running deionized water for 2 days and lyophilized. Different Gal-CH samples were synthesized by varying the feed ratio of LA to chitosan.

Gal-CH with a galactosylation degree of $10.3 \pm 0.39\%$ was used for the synthesis of galactosylated chitosan–polycaprolactone (Gal-CH–PCL). Polycaprolactone (PCL) was grafted onto chitosan based on a group-protection method with some modifications (Duan et al., 2010). Briefly, a given amount of Gal-CH was dissolved in 50 mL of methanesulfonic acid. To this solution, a prescribed amount of caprolactone monomer was introduced and the mixture was allowed to react at 45 °C for 12 h with stirring while purging with nitrogen. The mixture was filtrated and redispered in a solution containing 0.2 M KH_2PO_4 (200 mL), 10 M NaOH (30 mL) and some crushed ice to remove the acid residue. The precipitate was collected by filtration and dialyzed against running water for 2 days. After that, the product was lyophilized for further use. By mainly changing the weight ratio of caprolactone to Gal-CHs, several types of Gal-CH–PCL copolymers were synthesized using the same protocol. In addition, some chitosan–polycaprolactone (CH–PCL) copolymers without galactosylation were also synthesized with the same technique and they were used to prepare curcumin-loaded CH–PCL nanoparticles for controls.

2.3. Preparation of curcumin-loaded nanoparticles

Selected Gal-CH–PCLs were dissolved in 0.5% acetic acid to produce 0.15 wt% solution and a 0.5% stock solution of curcumin in ethanol was also prepared. In a typical procedure, to 30 mL of Gal-CH–PCL solution, a given volume of curcumin solution was added dropwise and well mixed. Afterwards, the mixture was slowly added with 20 mL of 0.07% sodium tripolyphosphate (TPP) solution with stirring at around 6000 rpm for ca. 30 min at 25 °C. The resulting nanoparticle suspension was centrifuged at 20,000 rpm for about 30 min, and the collected products were resuspended in water and washed until the pH became around 7.0. The obtained nanoparticles were then lyophilized at −75 °C for further measurements.

Different types of Gal-CH–PCL nanoparticles were prepared by using Gal-CH–PCLs containing various percentages of PCL component and changing the concentration of TPP solutions from 0.06 to 0.08%.

2.4. Characterization

Infrared (IR) spectra of different samples were recorded with a Nicolet Nexus 670 FT-IR spectrophotometer in transmission mode. Powder samples were prepared as KBr pellets and scanned against a blank KBr pellet background.

Chitosan and the selected Gal-CH or Gal-CH–PCL samples were dissolved in a mixed solvent of D_2O and CF_3COOD (95:5, v/v) to produce solutions with the same concentration at around 20 mg/mL. Each solution was introduced into a 5-mm NMR tube and ^1H NMR measurements were performed on a Bruker Avance 500 NMR spectrometer.

The content of C, H, and N in Gal-CHs was measured using an elemental analyzer (Vario EL III). The degree of galactosylation was calculated on the basis of elemental analysis. The weight percentage of PCL in Gal-CH–PCLs was also measured using an elemental analysis method.

The morphology of nanoparticles was viewed using a transmission electron microscope (TEM). Nanoparticles were suspended in deionized water to produce very dilute solutions, and the resulting solutions were sonicated so that the nanoparticles were in monodispersed state. A drop of nanoparticle suspension was placed onto carbon-coated copper TEM grid. After about 30 min of deposition, the grid was tapped with filter paper to remove surface water, negatively stained with 1% phosphotungstic acid for 5 min and allowed to dry at room temperature before loading in the microscope.

Hydrodynamic particle sizes of nanoparticles were measured using a Zetasizer Nano ZS90 instrument based on a quasi-elastic light scattering technique. A colloidal suspension of nanoparticles was prepared in ultra-pure water and sonicated for 1 min in an ice bath. The suspension was further diluted and the intensity of scattered light was detected at a scattering angle of 90° to an incident beam at a temperature of 25 °C. The size distribution of the nanoparticles is reported as a polydispersity index (PDI). The zeta potential (ζ) of nanoparticles was also measured on the same instrument.

2.5. Determination of encapsulation efficiency and loading efficiency

Encapsulation efficiency (EE) and loading efficiency (LE) of nanoparticles were determined following reported methods (Anitha et al., 2011a). Briefly, nanoparticle suspensions were first separated by centrifugation at 20,000 rpm for 30 min. They were washed with distilled water twice and then re-dispersed in ethanol and vortexed well. The yellowish supernatant was collected by centrifugation and assayed spectrophotometrically at 428 nm. EE of nanoparticles was calculated by following equation:

$$\mathrm{EE}\,(\%) = \frac{M_\mathrm{E}}{M_\mathrm{T}} \times 100\% \quad (1)$$

where M_E is the mass of curcumin encapsulated inside nanoparticles and M_T refers to totally added curcumin mass.

LE of the nanoparticles was calculated as follows:

$$\mathrm{LE}\,(\%) = \frac{M_\mathrm{E}}{M_\mathrm{N}} \times 100\% \quad (2)$$

where M_E is the mass of curcumin encapsulated inside nanoparticles, and M_N, the mass of nanoparticles.

2.6. In vitro release of curcumin

A PBS solution (pH 7.2) containing 0.5% Tween 80 and 10% ethanol was used as the release medium for release measurements of curcumin (Suwantong, Opanasopit, Ruktanonchai, & Supaphol, 2007). The medium was formulated on the basis of adequate solubility of the released curcumin while trying to use as much buffer as permissible (Chen et al., 2012). The nanoparticle suspension was centrifuged at 20,000 rpm for 40 min and the collected pellet was re-dispersed in the release buffer. The total volume of suspension was divided into a series of Eppendorf tubes with the same volume each, and all tubes were shaken at 37 °C and 70 rpm on an orbital shaking table. At predetermined time points, 1 mL of sample solution was withdrawn and an equal amount of fresh medium was refilled. The amount of curcumin in sample solutions was determined at 428 nm using a spectrophotometer.

2.7. Cell culture

Human hepatocellular carcinoma (HepG2) cells, human cervix epithelial carcinoma (HeLa) cells and human normal liver cells (L02 hepatocytes) were cultured in DMEM supplemented with 10% fetal bovine serum (FBS), streptomycin at 100 μg/mL and penicillin at 100 U/mL at 37 °C in a humidified atmosphere containing 5% CO_2. After incubating for a required period of time, the cells were washed off the culture flask using trypsin–EDTA, harvested by centrifugation and resuspended in the growth medium for further experiments.

2.8. Cellular uptake

The absorption spectrum of curcumin in the cell lysate can provide a comparative account for the amount of nanoparticles taken up by cells. Cells (HepG2 or HeLa) were seeded into 24-well plates with a density of 5×10^4 cells/well. After 24 h incubation in DMEM supplemented with 5% FBS, the cells in different wells were treated with equivalent dose (5, 10, and 15 μg/mL) of free curcumin and curcumin-loaded nanoparticles, respectively, and incubated for various periods up to 24 h. At each time point, the medium was removed and the cells were washed with PBS twice. To extract curcumin, the cells were trypsinized and lysed with ethanol using probe sonication at higher amplitude so that the curcumin inside the internalized nanoparticles were well extracted. The lysate was centrifuged at 12,000 rpm for 5 min, and supernatant containing ethanolic curcumin was quantified at 428 nm spectrophotometrically (Anitha et al., 2011b; Kunwar et al., 2008). Some HepG2 cells treated with free curcumin or curcumin-loaded nanoparticles for 6 h at an equivalent curcumin dose of 10 μg/mL were also viewed using fluorescence microscope.

2.9. Cell viability measurements

The cell viability was assessed using a MTT assay (Wan, Cao, Zhang, Wang, & Wu, 2008). Cells (HepG2 or L02) at a density of 1×10^4 cells/well were seeded in 96-well culture plates with RPMI1640 supplemented with 5% FBS. After 24 h incubation, the medium was replaced by the fresh medium and the cells were cultured for additional 24 h. After that, each well was refreshed with RPMI1640 supplemented with 5% FBS and added with an equivalent dose of free curcumin and curcumin-loaded nanoparticles at various curcumin amounts changing from 5 to 40 μg/mL. After 24 h incubation, each well was added with 20 μL of MTT (5 mg/mL) and incubated 4 h at 37 °C. The supernatant fluid was removed and 150 μL of dimethyl sulfoxide was added to each well to dissolve blue formazan precipitate. The absorbance of the solution was measured at 570 nm by using a microplate reader. RPMI1640 medium, HepG2 or L02 cells without nanoparticle treatment or with the treatment of blank Gal-CH–PCL nanoparticles were used as controls.

2.10. Apoptosis assay by flow cytometry

Cell apoptosis was assessed by detecting phosphatidyl serine exposure in HepG2 or L02 cells with an Annexin V-FITC and propidium iodide apoptosis analysis kit (BD Pharmingen) following a reported method (Anitha et al., 2011a). After reaching around 75% confluency, the cells were treated with various amounts of free curcumin and curcumin-loaded Gal-CH–PCL nanoparticles, respectively, and incubated in complete growth culture medium for various durations up to 72 h. At prescribed time intervals, the cells were harvested by trypsinization and washed with ice-cold PBS for 5 min at 4 °C. The supernatant was removed and the collected pellet was resuspended in ice-cold 1× binding buffer to 5×10^5–5×10^6 cells/mL. 5 μL of Annexin V-FITC solution and 2 μL of dissolved propidium iodide were added to 100 μL of the cell suspensions. The samples were mixed gently and incubated at room temperature for 15 min in the dark. After that, 400 μL of ice-cold 1× binding buffer was added, mixed gently, and the cells were analyzed by flow cytometry (BD FACSAria).

2.11. Statistical analysis

Analysis of variance was performed on the data using statistical software (SPSS 15.0 for Windows). The threshold for the level of statistical significance was set to $p < 0.05$.

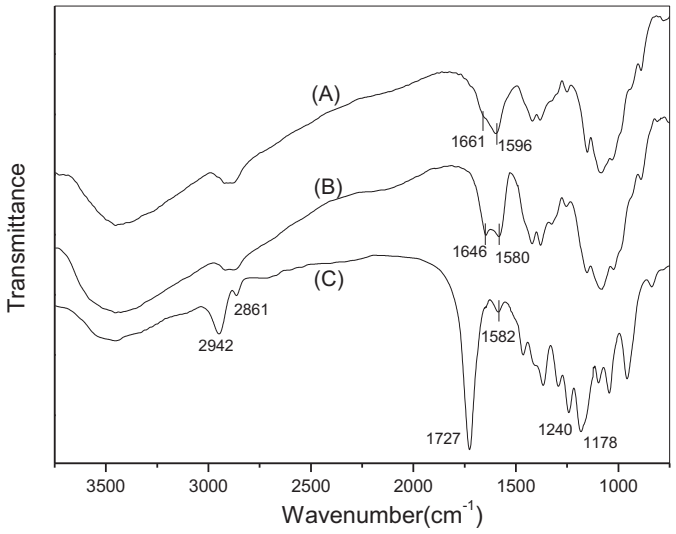

Fig. 1. IR spectra of chitosan (A), Gal-CH (B) (degree of galactosylation: 10.3%) and Gal-CH–PCL (C) (degree of galactosylation: 10.3% and PCL content in Gal-CH–PCL: 34.7 wt%).

3. Results and discussion

3.1. Synthesis of Gal-CH–PCL

Gal-CH–PCLs were synthesized via a two-step pathway by first galactosylating chitosan and then grafting the resulting Gal-CHs with PCL. In principle, PCL side chains can be grafted onto the C-2, C-3 or C-6 sites of chitosan backbone using various techniques (Gao et al., 2008; Wu et al., 2011). In the present study, PCL side chains were grafted onto the C-3 site or C-6 site of Gal-CH units using methanesulfonic acid as a reaction medium in considering that methanesulfonic acid is an effective protective reagent and a catalyst for the synthesis of chitosan–polycaprolactone (CH–PCL) (Duan et al., 2010). By doing so, the protonized amino groups at the C-2 site of Gal-CH units would get free after the deprotection and they can further be crosslinked by TPP.

Fig. 1 presents IR spectra of chitosan, Gal-CH and Gal-CH–PCL samples. In Fig. 1(A), a band at 1596 cm^{-1} is attributed to amino groups at the C-2 site of chitosan and a shoulder at round 1661 cm^{-1} is usually recorded for chitosan having a high deacetylation degree (Wan et al., 2004). With respect to the spectrum of Gal-CH shown in Fig. 1(B), a band at 1580 cm^{-1} should be ascribed to the residual primary amine of chitosan backbone with a small shift compared to the spectrum of chitosan, and a new band registered at around 1646 cm^{-1} indicates that some primary amine of chitosan backbone is changed into a secondary amine structure due to the reaction with LA. These bands are in basic agreement with reported results for Gal-CH (Gao et al., 2003). In Fig. 1(C), several new bands at 2942, 2861, 1727, 1240 and 1178 cm m^{-1} appeared in comparison to Fig. 1(A) and (B). These new peaks can be assigned to the characteristic absorption of ester structures for PCL side chains (Liu, Li, Fang, & Chen, 2005). In addition, Fig. 1(C) shows a peak located at around 1582 cm^{-1}, which corresponds to the originally residual amino groups in Gal-CHs, and thus, this peak should suggest that the amino groups at the C-2 site of Gal-CH chains are still well remained, and the PCL side chains are grafted onto the C-6 site or the C-3 site but not at the C-2 site of the Gal-CHs.

Fig. 2 shows ^{1}H NMR spectra of chitosan, Gal-CH and Gal-CH–PCL samples. In comparison to the spectrum of chitosan, the Gal-CH sample has several new peaks located at around 4.1, 4.2 and 4.5 ppm (see Fig. 2(B)). The peaks at ca. 4.1 and 4.2 ppm can be attributed to typical shifts of lactobionic acid and another peak at around 4.5 ppm is associated with —CONH—. Some reported results support similar ^{1}H NMR spectra for the presently synthesized Gal-CH (Feng & Dong, 2006; Kim et al., 2004). The spectrum in Fig. 2(B) should suggest that chitosan has been successfully galactosylated. It can be seen from Fig. 2(C) that the characteristic peaks of chitosan and LA are still remained while four new peaks at around 1.15, 1.35, 2.05, and 3.4 ppm are recorded. These new peaks can be ascribed to the PCL component due to presence of protons next to the carbonyl group of PCL side chains according to the analysis for CH–PCLs (Liu, Chen, & Fang, 2006). On the basis of IR and ^{1}H NMR spectra of the Gal-CH and Gal-CH–PCL samples, it can be reached that some PCL side chains have been successfully grafted on Gal-CH main chains.

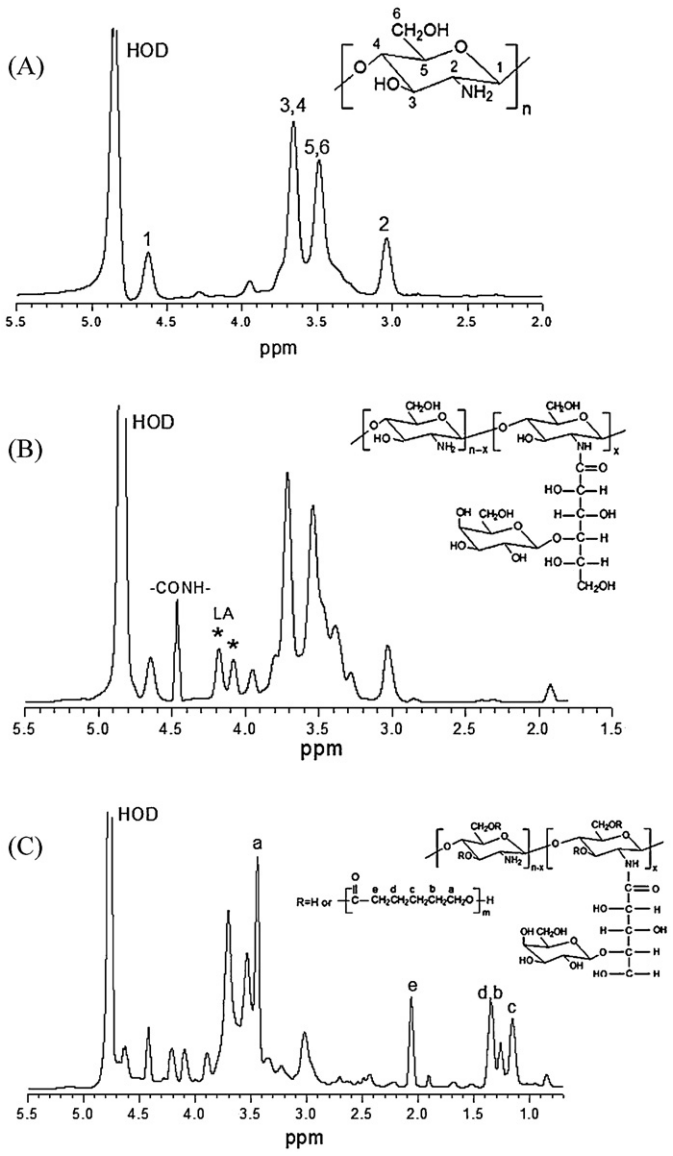

Fig. 2. ^{1}H NMR spectra of chitosan (A), Gal-CH (B) (degree of galactosylation: 10.3%) and Gal-CH–PCL (C) (degree of galactosylation: 10.3% and PCL content in Gal-CH–PCL: 34.7 wt%).

Lactobionic acid is a weak acid and is incapable of directly acylating chitosan. In the present instance, with the aid of the reactive intermediate O-acylurea, successful galactosylation reaction between amino groups of chitosan and lactobionic acid was achieved, which is confirmed by IR and NMR measurements. In considering the potential application of presently synthesized carriers, a higher degree of galactosylation (DG) for Gal-CHs seems to be favorable for enhanced hepatocyte-targeted functions because

Table 1
Parameters of curcumin-loaded nanoparticles.[a]

Nanoparticle sample	TPP concentration (%, w/v)	PCL content in Gal-CH–PCL (wt%)	Mean size (nm)	PDI	ζ (mV)	EE (%)	LE (%)
MP-I(1)[b]	0.06	–	158.2 ± 11.9	0.29 ± 0.08	30.7 ± 1.8	25.2 ± 2.4	1.43 ± 0.12
MP-I(2)	0.07	–	127.5 ± 10.5	0.23 ± 0.07	28.3 ± 1.5	29.3 ± 2.1	1.89 ± 0.11
MP-I(3)	0.08	–	109.7 ± 8.7	0.21 ± 0.05	26.6 ± 1.6	32.9 ± 2.5	2.16 ± 0.13
MP-II(1)	0.06	19.6 ± 2.1	193.8 ± 13.2	0.27 ± 0.09	27.4 ± 1.9	53.7 ± 2.7	4.18 ± 0.12
MP-II(2)	0.07	19.6 ± 2.1	134.6 ± 11.8	0.24 ± 0.06	25.1 ± 1.7	57.2 ± 2.1	4.56 ± 0.14
MP-II(3)	0.08	19.6 ± 2.1	116.4 ± 10.3	0.22 ± 0.07	23.2 ± 1.3	63.3 ± 3.3	4.97 ± 0.13
MP-III(1)	0.06	28.5 ± 2.3	212.6 ± 13.6	0.26 ± 0.06	24.9 ± 1.4	65.4 ± 2.8	5.24 ± 0.14
MP-III(2)	0.07	28.5 ± 2.3	162.5 ± 12.8	0.25 ± 0.08	22.6 ± 1.7	70.1 ± 2.6	5.65 ± 0.15
MP-III(3)	0.08	28.5 ± 2.3	124.3 ± 11.3	0.24 ± 0.05	21.3 ± 1.5	76.5 ± 3.2	6.07 ± 0.14
MP-IV(1)	0.06	38.2 ± 1.9	227.8 ± 13.7	0.23 ± 0.06	23.5 ± 1.8	73.8 ± 3.1	5.92 ± 0.15
MP-IV(2)	0.07	38.2 ± 1.9	189.4 ± 12.4	0.27 ± 0.08	20.8 ± 1.6	77.4 ± 2.9	6.23 ± 0.16
MP-IV(3)	0.08	38.2 ± 1.9	142.5 ± 11.6	0.28 ± 0.05	19.4 ± 1.8	82.2 ± 3.1	6.48 ± 0.15
MP-V(1)[c]	0.06	37.6 ± 2.2	236.1 ± 13.4	0.24 ± 0.06	24.7 ± 1.6	75.9 ± 2.9	6.04 ± 0.16
MP-V(2)	0.07	37.6 ± 2.2	195.2 ± 11.5	0.27 ± 0.08	20.1 ± 1.5	79.6 ± 3.2	6.37 ± 0.17
MP-V(3)	0.08	37.6 ± 2.2	148.7 ± 11.2	0.25 ± 0.07	19.3 ± 1.4	83.7 ± 2.7	6.56 ± 0.15

[a] Data in table: mean ± SD ($n = 4$); the concentration of solution for the preparation of all nanoparticles was fixed at 0.15% (w/v).
[b] Samples in set MP-I were prepared using Gal-CH without PCL grafting and they were used as control.
[c] Samples in set MP-V were prepared using CH–PCL without galactosylation and they were used as control.

the endocytosis of nanoparticles is partially operated by ligand-receptor interactions. Nevertheless, a high DG for Gal-CHs may not be encouraged since some optimal Gal-CHs had been used as hepatocyte-targeted cationic gene vectors where the DG for Gal-CHs was recommended as around 10% for effective endocytosis (Kim et al., 2004). Hence, some Gal-CHs with a DG of 10.3 ± 0.39% were adopted as starting materials for grafting polymerization of Gal-CH–PCLs even though various DGs up to around 14% for certain Gal-CHs can be achieved.

Although the weight percentage of PCL in the Gal-CH–PCLs could reach around 50 wt% under present reaction conditions, the PCL content in Gal-CH–PCLs should be controlled within a rational range because Gal-CH–PCLs with a higher PCL content are not well soluble in aqueous solvents and may result in poor fabrication of nanoparticles. Therefore, Gal-CH–PCLs with PCL content lower than 40 wt% were selected for producing curcumin-loaded Gal-CH–PCL nanoparticles.

3.2. Parameters of Gal-CH–PCL nanoparticles

Gal-CH–PCLs can be crosslinked using the same types of crosslinkers applicable to chitosan since many residual amino groups at the C-2 site of chitosan units in Gal-CH–PCLs are free. In the present study, TPP, a type of ionic crosslinker, was selected for crosslinking Gal-CH–PCL nanoparticles in consideration of its clinic safety because many commonly used covalent crosslinkers for chitosan, such as diisocyanate, epoxy compound and glutaraldehyde, can impair biocompatibility of the resulting nanoparticles. Fig. 3(A) presents a representative TEM image for Gal-CH–PCL nanoparticles prepared by using Gal-CH–PCL containing around 19 wt% of PCL, and the size-distribution of nanoparticles is presented in Fig. 3(B). The TEM image shows that these nanoparticles had various sizes changing from several tens of nanometers to about 200 nm. Fig. 3(B) indicates that the size of nanoparticles had an approximate Gaussian distribution and the average size of nanoparticles was around 130 nm. It was found that the PCL content in Gal-CH–PCLs, the concentration of Gal-CH–PCL solutions and the used amount of TPP acted as three key factors for modulating the morphology and properties of Gal-CH–PCL nanoparticles. By keeping the concentration of Gal-CH–PCL solutions constant (0.15% (w/v)) and changing the PCL content in Gal-CH–PCLs or the used amount of TPP, several types of nanoparticles were produced and relevant parameters for them are summarized in Table 1. Some curcumin-loaded nanoparticles were also prepared using Gal-CHs without PCL grafting or CH–PCLs

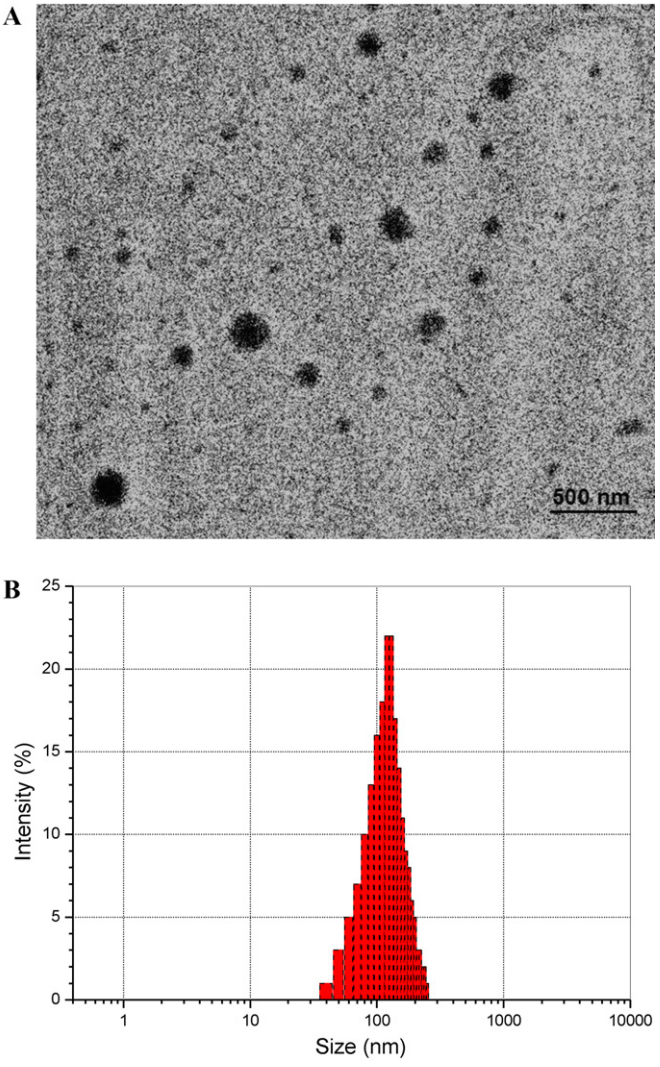

Fig. 3. TEM micrograph (A) and size-distribution (B) of Gal-CH–PCL nanoparticles (PCL content in Gal-CH–PCL: 19.6 wt%; concentration of Gal-CH–PCL solution: 0.15% and TPP concentration: 0.07%).

without galactosylation under the same processing conditions and they were used as controls.

It has also been reported that nanoparticles having larger sizes, for example, greater than 250 nm, hardly reach the liver parenchymal cells whereas smaller nanoparticles have an increasing potential to accumulate at the hepatic tumor site (Acharya & Sahoo, 2011; Das et al., 2009). On the other hand, to ensure efficient endocytosis, nanoparticles should be big enough to prevent themselves from rapidly leaking into capillary blood vessels or to escape from the capture stemmed from macrophages that lodge in the reticuloendothelial system (Acharya & Sahoo, 2011; Litzinger, Buiting, Rooijen, & Huang, 1994). The size of nanoparticles was thus regulated in such a way that the mean size of nanoparticles was larger than 100 nm but smaller than 250 nm.

Table 1 shows that mean size of nanoparticles in each set significantly decreased with increasing TPP amounts, and on the other hand, the PCL content in Gal-CH–PCLs or in CH–PCLs also regulated the mean size of nanoparticles to a certain extent when fixing the amount of TPP. These results suggest that the size of nanoparticles can be efficiently controlled by changing the used amount of TPP.

Table 1 points out that these nanoparticles had their PDI less than 0.3, revealing their relatively narrow size-distributions. In general, the charge on the surface of nanoparticles can act as an important factor to influence the stability of nanoparticle suspension as well as the interactions between nanoparticles and the targeted cell membrane. Data in Table 1 show that these nanoparticles had positive zeta potential changing from around 20 to 30 mV, which should be ascribed to the positive charge arisen from chitosan units. In the case of set MP-I, the positive zeta potential for nanoparticles was attributed to the direct contribution of amino groups in chitosan units. With respect to sets MP-II, MP-III and MP-IV, the corresponding positive zeta potential could be resulted from the residual amino groups in chitosan units. In the present case, Gal-CH–PCLs are amphiphilic polymers, and hence, the hydrophilic chitosan chains could stretch outward and form the outer layer of nanoparticles during the fabrication of nanoparticles because these nanoparticles were prepared using aqueous media. As a result, positive charges derived from residual amino groups in the chitosan backbone would contribute to the zeta potential of the Gal-CH–PCL nanoparticles. Table 1 also signifies that zeta potential of nanoparticles in each set slightly decreased with increasing amount of TPP. This characteristic may be ascribed to the fact that a certain amount of residual amino groups on the Gal-CH–PCL chains was consumed due to the ionic crosslinking correlated to TPP, leading to decreased net positive charges on the surface of nanoparticles. In addition, it can also be noticed that zeta potential of nanoparticles slightly decreased with increasing PCL content in the Gal-CH–PCLs in each set of nanoparticles. As shown in Table 1, the increasing PCL content in the Gal-CH–PCLs would result in increased mean size, which may thus increase the surface area of single nanoparticle, and in turn, decrease the charge density on the surface, leading to slightly decreasing zeta potential. Data for zeta potential reveal that presently prepared nanoparticles should be relatively stable and they might also be favorable for delivering the encapsulated curcumin due to the potential interactions between the positively charged surface of nanoparticles and negatively charged cell membranes.

Table 1 exhibits that in comparison to the sample in set MP-I, the corresponding one in sets MP-II, MP-III and MP-IV had significantly higher EE and LE ($p < 0.01$); and on the other hand, the sample in set MP-V had very similar EE and LE compared to the matched one in the set MP-IV. In addition, an increase in PCL content in the Gal-CH–PCLs also resulted in increasing EE and LE, suggesting that the PCL content in the Gal-CH–PCLs can play an important role for encapsulating curcumin. These results are reasonable because Gal-CH–PCLs were amphiphilic and the resulting

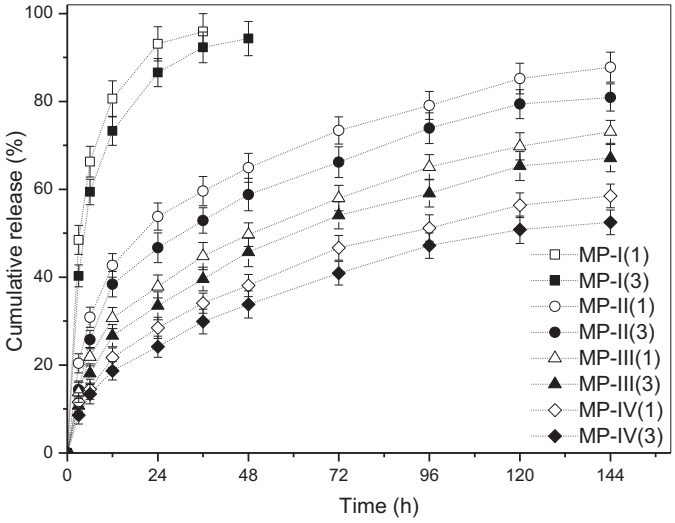

Fig. 4. Release patterns of curcumin from different nanoparticles (see Table 1).

Gal-CH–PCL nanoparticles should have a hydrophobic interior due to the fabrication of nanoparticles in aqueous media. As a result, the hydrophobic interior of Gal-CH–PCL nanoparticles were able to entrap hydrophobic curcumin more effectively compared to those nanoparticles prepared with Gal-CHs that did not contain any PCL component (e.g., samples in set MP-I). For the nanoparticles in sets MP-II, MP-III and MP-IV, the increasing PCL content in Gal-CH–PCLs could also increase the ratio of hydrophobic interior volume to the integral volume of the nanoparticles, leading to increasing EE and LE for these nanoparticles.

3.3. *In vitro release of curcumin*

In general, the drug release from nano-size carriers depends upon many variables (Chan et al., 2009). In the present instance, the Gal-CH–PCL composition and the amount of TPP were selected as two variables and their effect on the release behavior of Gal-CH–PCL nanoparticles was mainly investigated because these two variables were found to be crucial for modulating the curcumin release.

Release profiles of some samples selected from sets MP-I, MP-II, MP-III and MP-IV were examined and relevant results are represented in Fig. 4. Of them, the nanoparticle samples in set MP-I were used as controls. To see the effect of PCL content in Gal-CH–PCLs on the release behavior of nanoparticles, the release patterns for MP-II(3), MP-III(3) and MP-IV(3) were compared. The plot for MP-I(3) nanoparticles shows that they had a very fast release rate in the first day, followed by a slowdown until the cumulative release reached a level higher than 95%. In contrast to this observation, MP-II(3) nanoparticles had greatly reduced initial burst in the first day, and after that, they exhibited an approximately constant release rate until day 5. As indicated in Table 1, both MP-I(3) and MP-II(3) nanoparticles had similar mean-size, PDI and ζ, and a main difference between them was that MP-I(3) nanoparticles were prepared using the Gal-CH that was not grafted with any PCL component whereas MP-II(3) nanoparticles were prepared using the Gal-CH–PCL containing around 19 wt% of PCL component. In the case of MP-II(3) nanoparticles, the relatively rigid and hydrophobic PCL side chains in Gal-CH–PCL(a) may function as hook-like branches to drag the entrapped curcumin molecules and hinder them from diffusing cross the surface of nanoparticles, resulting in significantly reduced initial burst and subsequently delayed release as compared to MP-I(3) nanoparticles. Fig. 4 also shows that the release profiles of MP-III(3) and MP-IV(3) nanoparticles

were quite similar to that of MP-II(3) nanoparticles but with further reduced initial burst and a slowdown in their release rate in comparison to MP-II(3) nanoparticles. As shown in Table 1, the PCL content in the Gal-CH–PCL for MP-III(3) or MP-IV(3) nanoparticles was significantly higher than that for MP-II(3) nanoparticles, as a consequence, MP-III(3) and MP-IV(3) nanoparticles would have enhanced ability to hold the encapsulated curcumin, leading to significantly reduced initial burst and subsequently decreased release rates.

The plots in Fig. 4 illustrate that in each set, although two types of nanoparticles had a large difference in the TPP concentration (see Table 1) the effect of crosslinker on the release patterns of the nanoparticles was insignificant ($p > 0.05$), and the concentration of crosslinker only slightly regulated the release rates. In the present study, Gal-CH–PCL nanoparticles were crosslinked by TPP through ionic linkages, and meanwhile, the surface of nanoparticles should be hydrophilic due to the manufacture of nanoparticles in aqueous media. Therefore, Gal-CH–PCL nanoparticles could become quite swollen when they were exposed to release media so that the increasing amount of TPP was not able to impose a strong impact on the swollen and looses three-dimensional network inside the nanoparticles, resulting in insignificant changes in the release patterns of nanoparticles.

Based on above observations, it can be concluded that the release behavior of Gal-CH–PCL nanoparticles was governed by the PCL content in Gal-CH–PCLs instead of the concentration of TPP solutions used. Additionally, results presented in Table 1 and Fig. 4 should suggest that the nanoparticles in set MP-I are unsuitable for delivering curcumin due to their low EE and LE as well as fast release rate. The nanoparticles in set MP-I were therefore excluded for further investigations.

3.4. Cell uptake study

MP-II(3), MP-III(3) and MP-IV(3) nanoparticles were selected for measuring their cellular uptake while free curcumin and MP-V(3) nanoparticles without galactosylation were used as controls to find out whether PCL content in Gal-CH–PCLs or galactosylation would significantly influence the cellular uptake. The cellular uptake in HeLa cells versus equivalent curcumin concentration is presented in Fig. 5(A). In comparison with free curcumin, cellular uptake values for different types of nanoparticles were significantly higher ($p < 0.01$). It has been reported that curcumin-encapsulated nanoparticles can be much more efficiently internalized by HeLa cells or pancreatic cells compared to free curcumin (Mohanty & Sahoo, 2010). Fig. 5(A) suggests that the presently synthesized CH–PCL copolymers with or without galactosylation are able to enhance internalization of the resulting nanoparticles, and thus, they may function as effective carriers to transport the entrapped curcumin into HeLa cells and possibly improve the bioavailability of curcumin.

Fig. 5(A) also exhibits that there were no significant differences in the cellular uptake ($p > 0.05$) among MP-II(3), MP-III(3), MP-IV(3) and MP-V(3) nanoparticles. It is known that HeLa cells do not have any asialoglycoprotein (ASGP) receptors (Park et al., 2000), and thus, it is reasonable to believe that there were no specific interactions between these nanoparticles and HeLa cells via a ligand-receptor pathway even though MP-II(3), MP-III(3) and MP-IV(3) nanoparticles had some galactose ligands on their surface. Therefore, these nanoparticles could be internalized into HeLa cells mainly by interactions between the surface of nanoparticles and the cell membrane of HeLa cells via a passive entrapping mechanism. As indicated in Table 1, although MP-II(3), MP-III(3) and MP-IV(3) nanoparticles were produced by using different Gal-CH–PCLs with various PCL percentages, there were small differences in their main parameters such as mean size, PDI, ζ, EE and LE. As a result, these nanoparticles were likely internalized into HeLa cells with almost similar endocytosis probability and efficiency.

Fig. 5(B) represent the corresponding cellular uptake for MP-II(3), MP-III(3), MP-IV(3) and MP-V(3) nanoparticles in HepG2 cells. In this instance, several points can be drawn: (1) dependence of cellular uptake on the equivalent curcumin concentration was still registered; (2) MP-V(3) nanoparticles had higher cellular uptake values than free curcumin; and (3) MP-II(3), MP-III(3) and MP-IV(3) nanoparticles exhibited significantly higher cellular uptake than MP-V(3) nanoparticles.

It has been reported that when ASGP receptor-matched ligands on the surface of nanoparticle carriers are bound to the ASGP receptor of hepatocytes, the ligand-receptor complex can be rapidly internalized by the cells, and the receptor will recycle back to the surface of hepatocytes for the subsequent ligand bonding (Mi et al., 2007). In the present case, HepG2 cells bear ASGP receptors (Park et al., 2000), and hence, the higher uptake values for MP-II(3), MP-III(3) and MP-IV(3) nanoparticles can be ascribed to the interactions between the ASGP receptors on HepG2 cells and the galactose ligands on the surface of nanoparticles. On the other hand, MP-V(3) nanoparticles were prepared using CH–PCL (see Table 1) and did not have any galactose residues on their surfaces, and they should be still internalized into HepG2 cells via a passive entrapping pathway.

Cellular uptake for some curcumin-loaded nanoparticles in HepG2 cells were also viewed using fluorescence microscope in consideration of fluorescent properties of curcumin. Fig. 5(C) shows some representative fluorescence images obtained from HepG2 cells treated with free curcumin and curcumin-loaded nanoparticles. These images reveal that under the same incubation conditions, a very small amount of free curcumin was internalized; a higher amount of curcumin was delivered into HepG2 cells by using MP-V(3) nanoparticles in comparison to free curcumin; and MP-II(3) and MP-IV(3) nanoparticles were capable of transporting curcumin into HepG2 cells with further increased efficiency compared to free curcumin or MP-V(3) nanoparticles. These results are in basic agreement with those presented in Fig. 5(B).

Fig. 5(B) and (C) confirms that Gal-CH–PCL nanoparticles can deliver curcumin to the HepG2 cells with specifically targeted characteristics, and with the aid of some optimal Gal-CH–PCL nanoparticles, a significant increase in curcumin internalization toward HepG2 cells can be achieved compared to free curcumin, suggesting that the bioavailability of curcumin in HepG2 cells could be significantly increased using presently synthesized Gal-CH–PCL carriers.

Table 1 shows that MP-III(3) and MP-IV(3) nanoparticles had similar parameters with small differences, and meanwhile, Fig. 4 indicates that MP-III(3) nanoparticles showed medium-speed release behavior compared to MP-II(2) or MP-IV(3) nanoparticles. Accordingly, MP-III(3) nanoparticles were selected for further examining their effect on the viability of HepG2 cells.

3.5. Cell viability

Considering that MP-III(3) nanoparticles were prepared using Gal-CH–PCL containing about 28 wt% of PCL (see Table 1), some blank Gal-CH–PCL nanoparticles without curcumin-load were also prepared under the same processing conditions that were applied to MP-III(3) nanoparticles and used as controls. The mean-size, PDI and ζ value of blank Gal-CH–PCL nanoparticles were measured as 136.5 ± 10.7 (nm), 0.22 ± 0.06 and 28.9 ± 2.3 (mV), respectively, which are very similar to those for MP-III(3) nanoparticles (see Table 1).

The blank Gal-CH–PCL nanoparticles were first examined for their effect on the viability of HepG2 or L02 cells and relevant results in comparison to the nontoxic control are represented in Fig. 6(A). The bar-graphs in Fig. 6(A) show that more than 90% of

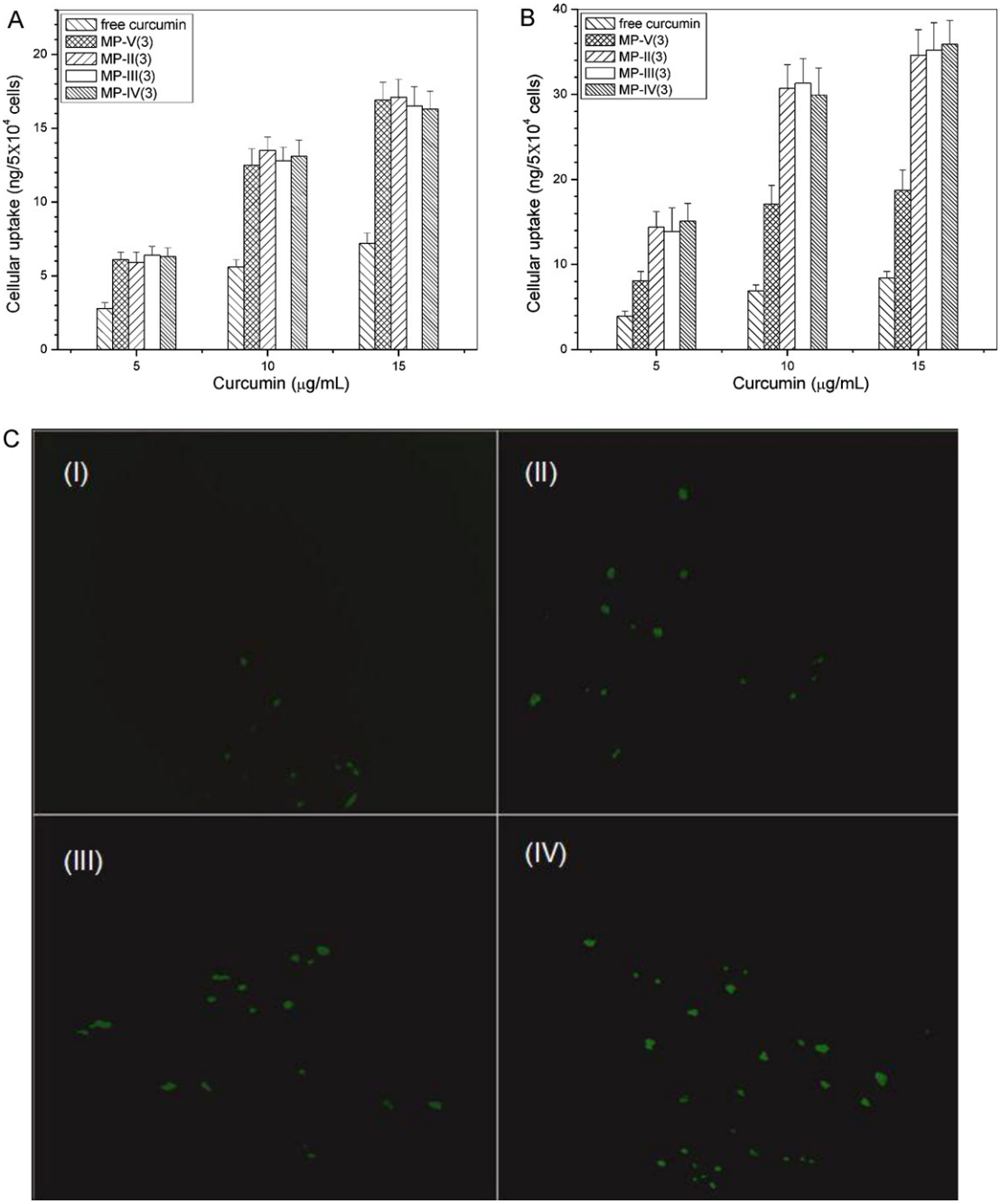

Fig. 5. Cellular uptake in HeLa cells (A) and in HepG2 cells (B) (incubation time: 24 h, equivalent curcumin dose: 10 μg/mL). Fluorescence images of cellular uptake in HepG2 cells (C) (incubation time: 6 h, equivalent curcumin dose: 10 μg/mL, original magnification: 40×; (I) free curcumin, (II) MP-V(3) nanoparticles, (III) MP-II(3) nanoparticles and (IV) MP-IV(3) nanoparticles).

the cells remained viable during the period of incubation within the measurement range, confirming that the blank Gal-CH–PCL nanoparticles in an amount less than 400 μg/mL are nearly non-toxic to HepG2 or L02 cells, and they only imposed very limited cytotoxic impacts on HepG2 or L02 cells when the concentration of nanoparticles was higher than 400 μg/mL.

The effect of free curcumin and MP-III(3) nanoparticles on the viability of HepG2 or L02 cells is presented in Fig. 6(B). It can be seen that the viability of HepG2 cells decreased from around 80% to 15% or 24%, respectively corresponding to MP-III(3) nanoparticles and free curcumin when the equivalent curcumin dose altered from 10 to 40 μg/mL. On the other hand, the viability of L02 cells varied from around 95% to 49% or 54% in response to MP-III(3) nanoparticles and free curcumin, respectively, in the same measurement range. These results indicate that at a lower equivalent curcumin dose used, for example, 20 μg/mL or lesser, the overwhelming majority of L02 cells with treatments remained viable whereas the growth of HepG2 cells with the same treatment was already inhibited to a certain extent. In contrast to these observations, at higher equivalent curcumin doses that change from 20 to 40 μg/mL, both L02 and HepG2 cells had significantly decreased viability. In addition, it can also be seen that MP-III(3) nanoparticles had increasing ability to inhibit the growth of HepG2 cells compared to free curcumin when equivalent curcumin doses changed from 20 to 40 μg/mL. The enhanced ability of MP-III(3) nanoparticles for inhibiting the growth of HepG2 cells may be assigned to

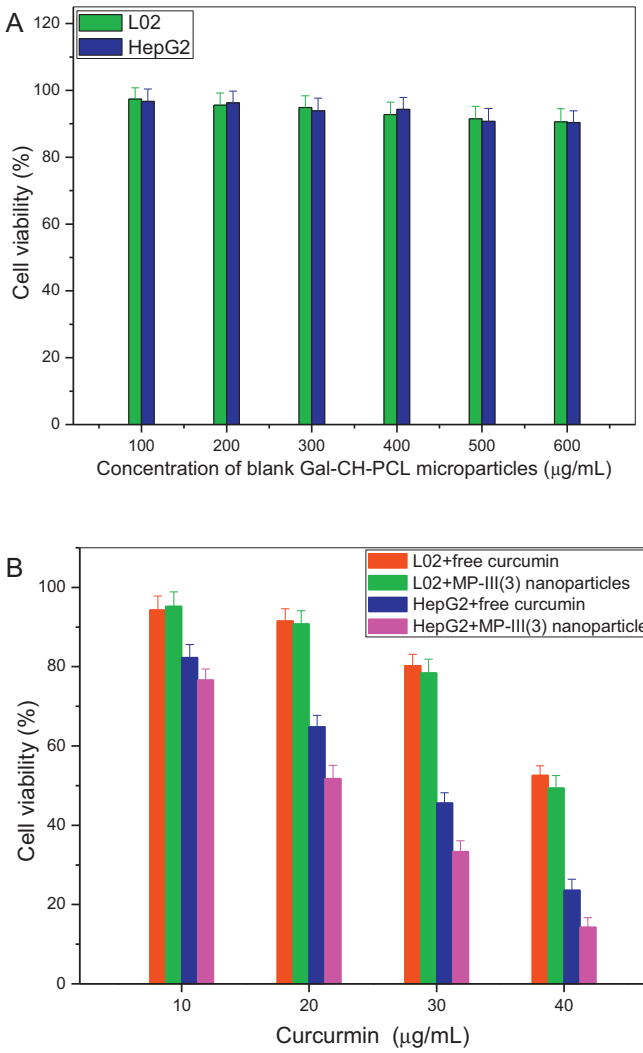

Fig. 6. Viability of HepG2 and L02 cells (24 h incubation). (A) Treatment with blank Gal-CH–PCL nanoparticles, and (B) treatment with free curcumin and MP-III(3) nanoparticles.

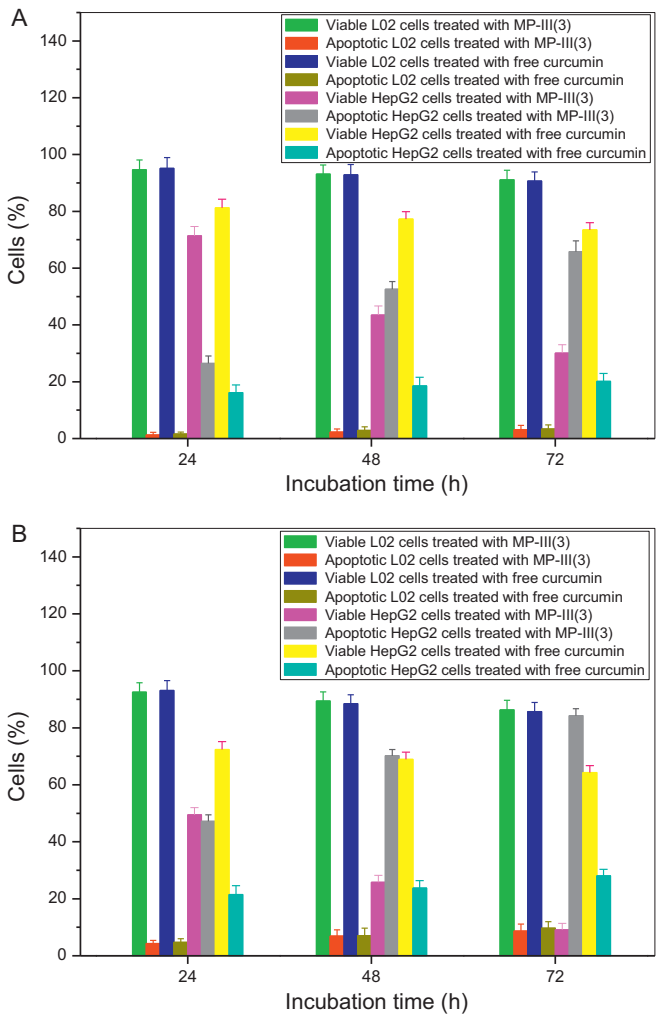

Fig. 7. Apoptosis of HepG2 and L02 cells after being treated with various equivalent curcumin doses of 10 μg/mL (A) and 20 μg/mL (B) for different periods of incubation time.

the higher cellular uptake of MP-III(3) nanoparticles in comparison to free curcumin, and MP-III(3) nanoparticles should transport more entrapped curcumin into HepG2 cells and release them thereafter. These results suggest that the anticancer activity of entrapped curcumin inside the MP-III(3) nanoparticles can be well retained while the cytotoxicity of curcumin to normal hepatocytes could be avoided if the equivalent curcumin dose is controlled at 20 μg/mL or lesser. In fact, some reports also indicate that at an equivalent curcumin dose of about 18 μg/mL, the exposed HepG2 cells would become apoptosis depending on the exposed time (Kunwar et al., 2008; Syng-ai, Kumari, & Khar, 2004). In the present instance, the equivalent curcumin dose was selected as 10 and 20 μg/mL in the subsequent investigations in considering safety of curcumin dose for normal liver cells.

3.6. Apoptosis analysis

It is known that Annexin V (AV) can efficiently bind to phosphatidyl serine that is usually exposed by flipping from the inner to the outer layer of plasma membrane during the early apoptosis of cells; and on the other hand, propidium iodide (PI) is a nuclear reagent that can stain necrotic cells. Certain groups of HepG2 or L02 cells incubated with various equivalent curcumin doses for different periods were detected using flow-cytometer, and the results are represented in Fig. 7(A) and (B), respectively.

Fig. 7(A) shows that with varied treatments of nanoparticles or free-curcumin up to 72 h, most L02 cells were still viable, and meanwhile, the number of viable HepG2 cells with the same treatments was much lower than that of L02 cells. In addition, it is also observed that apoptotic HepG2 cells treated with MP-III(3) nanoparticles were more than two times of that treated with free-curcumin after treatment for 72 h. Fig. 7(B) exhibits that more than 85% of exposed L02 cells was viable and only a small quantity of apoptotic L02 cells was measured after treatment with an equivalent curcumin dose of 20 μg/mL for 72 h. In the case of HepG2 cells, more cells became apoptotic in both free-curcumin-treated and MP-III(3)-treated groups compared to the matched one represented in Fig. 7(A). In particular, after 72 h incubation, the number of viable HepG2 cells treated with free curcumin was more than 6-fold higher than that treated with MP-III(3) nanoparticles. These results suggest that at a same equivalent curcumin dose within the safe dose range, the curcumin-loaded Gal-CH–PCL nanoparticles have a remarkably enhanced ability to induce apoptosis and necrosis of sensitized HepG2 cells in comparison to free curcumin, and during a prolonged treatment, the bioavailability of curcumin can be greatly improved by using present synthesized Gal-CH–PCLs.

4. Conclusions

Gal-CH–PCLs were successfully synthesized by a two-step method. Curcumin-loaded Gal-CH–PCL nanoparticles prepared with Gal-CH–PCLs having a galactosylation degree of around 10% and a PCL percentage less than 40 wt% could function as promising carriers with high initial load for delivering curcumin in a well controlled manner, and the PCL content in the Gal-CH–PCLs instead of the amount of crosslinker was found to be a key factor for governing the in vitro release behavior of the nanoparticles. The hepatocyte-targeted characteristic of Gal-CH–PCL nanoparticles was confirmed by the cell uptake using HepG2 cells. It was found that in comparison to free curcumin, the entrapped curcumin inside the nanoparticles still well retained its anticancer activity. Within a relatively safe range of equivalent curcumin doses, the Gal-CH–PCL nanoparticles had a remarkably enhanced ability to induce apoptosis of sensitized HepG2 cells in comparison to free curcumin, and during a prolonged treatment up to 72 h, apoptosis and necrosis rate of HepG2 cells treated with optimized Gal-CH–PCL nanoparticles could reach to a magnitude 6-fold higher than that treated with free curcumin. The results suggest that these Gal-CH–PCL nanoparticles can function as promising carriers for hepatocyte-targeted delivery of curcumin with greatly improved bioavailability.

Acknowledgement

This work was supported by the National Natural Science Foundation of China (Grant No. 81071470).

References

Acharya, S., & Sahoo, S. K. (2011). PLGA nanoparticles containing various anticancer agents and tumour delivery by EPR effect. *Advanced Drug Delivery Reviews*, *63*, 170–183.

Aggarwal, B. B., Kumar, A., & Bharti, A. C. (2003). Anticancer potential of curcumin: Preclinical and clinical studies. *Anticancer Research*, *23*, 363–398.

Aggarwal, B. B., & Sung, B. (2009). Pharmacological basis for the role of curcumin in chronic diseases: An age-old spice with modern targets. *Trends in Pharmacological Sciences*, *30*, 85–94.

Agnihotri, S. A., Mallikarjuna, N. N., & Aminabhavi, T. M. (2004). Recent advances on chitosan-based micro- and nanoparticles in drug delivery. *Journal of Controlled Release*, *100*, 5–28.

Anand, P., Kunnumakkara, A. B., Newman, R. A., & Aggarwal, B. B. (2007). Bioavailability of curcumin: Problems and promises. *Molecular Pharmacology*, *4*, 807–818.

Anand, P., Thomas, S. G., Kunnumakkara, A. B., Sundaram, C., Harikumar, K. B., Sung, B., et al. (2008). Biological activities of curcumin and its analogues (Congeners) made by man and mother nature. *Biochemical Pharmacology*, *76*, 1590–1611.

Anitha, A., Maya, S., Deepa, N., Chennazhi, K. P., Nair, S. V., Tamur, H., et al. (2011). Efficient water soluble O-carboxymethyl chitosan nanocarrier for the delivery of curcumin to cancer cells. *Carbohydrate Polymers*, *83*, 452–461.

Anitha, A., Deepagan, V. G., Divya Rani, V. V., Menon, D., Nair, S. V., & Jayakumar, R. (2011). Preparation, characterization, in vitro drug release and biological studies of curcumin loaded dextran sulphate-chitosan nanoparticles. *Carbohydrate Polymers*, *84*, 1158–1164.

Chan, J. M., Zhang, L., Yuet, K. P., Liao, G., Rhee, J. W., Langer, R., et al. (2009). PLGA-lecithin-PEG core-shell nanoparticles for controlled drug delivery. *Biomaterials*, *30*, 1627–1634.

Chen, H., Yang, W., Chen, H., Liu, L., Gao, F., Yang, X., et al. (2009). Surface modification of mitoxantrone-loaded PLGA nanospheres with chitosan. *Colloids and Surfaces B: Biointerfaces*, *73*, 212–218.

Chen, Y., Wu, Q., Zhang, Z., Yuan, L., Liu, X., & Zhou, L. (2012). Preparation of curcumin-loaded liposomes and evaluation of their skin permeation and pharmacodynamics. *Molecules*, *17*, 5972–5987.

Das, M., Mohanty, C., & Sahoo, S. K. (2009). Ligand-based targeted therapy for cancer tissue. *Expert Opinion on Drug Delivery*, *6*, 285–304.

Das, R. K., Kasoju, N., & Bora, U. (2010). Encapsulation of curcumin in alginate–chitosan–pluronic composite nanoparticles for delivery to cancer cells. *Nanomedicine: Nanotechnology, Biology and Medicine*, *6*, 153–160.

Duan, K., Chen, H., Huang, J., Yu, J., Liu, S., Wang, D., et al. (2010). One-step synthesis of amino-reserved chitosan-graft-polycaproctone as a promising substance of biomaterial. *Carbohydrate Polymers*, *80*, 498–503.

Feng, H., & Dong, C. (2006). Preparation and characterization of chitosan-graft-poly(ε-caprolactone) with an organic catalyst. *Journal of Polymer Science Part A: Polymer Chemistry*, *44*, 5353–5361.

Ganta, S., Devalapally, H., Shahiwala, A., & Amiji, M. (2008). A review of stimuli-responsive nanocarriers for drug and gene delivery. *Journal of Controlled Release*, *126*, 187–204.

Gao, K., Li, G., Shi, H., Lu, X., Gao, Y., & Xu, B. (2008). Synthesis and aggregation behavior of chitooligosaccharide-based biodegradable graft copolymers. *Journal of Polymer Science Part A: Polymer Chemistry*, *46*, 4889–4904.

Gao, S., Chen, J., Xu, X., Ding, Z., Yang, Y., Hua, Z., et al. (2003). Galactosylated low molecular weight chitosan as DNA carrier for hepatocyte-targeting. *International Journal of Pharmaceutics*, *255*, 57–68.

Greco, F., & Vicent, M. J. (2009). Combination therapy: Opportunities and challenges for polymer–drug conjugates as anticancer nanomedicines. *Advanced Drug Delivery Reviews*, *61*, 1203–1213.

Kim, T. H., Park, I. K., Nah, J. W., Choi, Y. J., & Cho, C. S. (2004). Galactosylated chitosan/DNA nanoparticles prepared using water-soluble chitosan as a gene carrier. *Biomaterials*, *25*, 3783–3792.

Kumar, M. N. V. R., Muzzarelli, R. A. A., Muzzarelli, C., Sashiwa, H., & Domb, A. J. (2004). Chitosan chemistry and pharmaceutical perspectives. *Chemical Reviews*, *104*, 6017–6084.

Kunwar, A., Barik, A., Mishra, B., Rathinasamy, K., Pandey, R., & Priyadarshini, K. I. (2008). Quantitative cellular uptake, localization and cytotoxicity of curcumin in normal and tumor cells. *Biochimica et Biophysica Acta*, *1780*, 673–679.

Liang, H. F., Chen, C. T., Chen, S. C., Kulkarni, A. R., Chiu, Y. L., Chen, M. C., et al. (2006). Paclitaxel-loaded poly(g-glutamic acid)–poly(lactide) nanoparticles as a targeted drug delivery system for the treatment of liver cancer. *Biomaterials*, *27*, 2051–2059.

Litzinger, D. C., Buiting, A. M. J., Rooijen, N., & Huang, L. (1994). Effect of liposome size on the circulation time and intraorgan distribution of amphipathic poly(ethylene glycol)-containing liposomes. *Biochimica et Biophysica Acta*, *1190*, 99–107.

Liu, L., Li, Y., Fang, Y., & Chen, L. (2005). Microwave-assisted graft copolymerization of ε-caprolactone onto chitosan via the phthaloyl protection method. *Carbohydrate Polymers*, *60*, 351–356.

Liu, L., Chen, L., & Fang, Y. (2006). Self-catalysis of phthaloylchitosan for graft copolymerization of ε-caprolactone with chitosan. *Macromolecular Rapid Communications*, *27*, 1988–1994.

Lu, P. L., Chen, Y. C., Ou, T. W., Chen, H. H., Tsai, H. C., Wen, C. J., et al. (2011). Multifunctional hollow nanoparticles based on graft-diblock copolymers for doxorubicin delivery. *Biomaterials*, *32*, 2213–2221.

Mi, F. L., Wu, Y. Y., Chiu, Y. L., Chen, M. C., Sung, H. W., Yu, S. H., et al. (2007). Synthesis of a novel glycoconjugated chitosan and preparation of its derived nanoparticles for targeting HepG2 cells. *Biomacromolecules*, *8*, 892–898.

Mohanty, C., & Sahoo, S. K. (2010). The in vitro stability and in vivo pharmacokinetics of curcumin prepared as an aqueous nanoparticulate formulation. *Biomaterials*, *31*, 6597–6611.

Muzzarelli, R. A. A. (2009). Chitins and chitosans for the repair of wounded skin, nerve, cartilage and bone. *Carbohydrate Polymers*, *76*, 167–182.

Muzzarelli, R. A. A., Greco, F., Busilacchi, A., Sollazzo, V., & Gigante, A. (2012). Chitosan, hyaluronan and chondroitin sulfate in tissue engineering for cartilage regeneration: A review. *Carbohydrate Polymers*, *89*, 723–739.

Park, I. K., Park, Y. H., Shin, B. A., Choi, E. S., Kim, Y. R., Akaike, T., et al. (2000). Galactosylated chitosan-graft-dextran as hepatocyte-targeting DNA carrier. *Journal of Controlled Release*, *69*, 97–108.

Suwantong, O., Opanasopit, P., Ruktanonchai, U., & Supaphol, P. (2007). Electrospun cellulose acetate fiber mats containing curcumin and release characteristic of the herbal substance. *Polymer*, *48*, 7546–7557.

Syng-ai, C., Kumari, A. L., & Khar, A. (2004). Effect of curcumin on normal and tumor cells: Role of glutathione and bcl-2. *Molecular Cancer Therapeutics*, *3*, 1101–1108.

Wang, S. N., Deng, Y. H., Xu, H., Wu, H. B., Qiu, Y. K., & Chen, D. W. (2006). Synthesis of a novel galactosylated lipid and its application to the hepatocyte-selective targeting of liposomal doxorubicin. *European Journal of Pharmaceutics and Biopharmaceutics*, *62*, 32–38.

Wan, Y., Creber, K. A. M., Peppley, B., & Bui, V. T. (2004). Ionic conductivity and tensile properties of hydroxyethyl and hydroxypropyl chitosan membranes. *Journal of Polymer Science Part B: Polymer Physics*, *42*, 1379–1397.

Wan, Y., Cao, X., Zhang, S., Wang, S., & Wu, Q. (2008). Fibrous poly(chitosan-g-DL-lactic acid) scaffolds prepared via electro-wet-spinning. *Acta Biomaterialia*, *4*, 876–886.

Wu, H., Zhang, J., Xiao, B., Zan, X., Gao, J., & Wan, Y. (2011). N-(2-hydroxypropyl)-3-trimethylammonium chitosan-poly(ε-caprolactone) copolymers and their antibacterial activity. *Carbohydrate Polymers*, *83*, 824–830.

Wu, J., Nantz, M. H., & Zern, M. A. (2002). Targeting hepatocytes for drug and gene delivery: Emerging novel approaches and application. *Frontiers in Bioscience*, *7*, 717–725.